Saccharide–RNA recognition in an aminoglycoside antibiotic–RNA aptamer complex

Licong Jiang, Asif K Suri, Radovan Fiala and Dinshaw J Patel

Background: Aminoglycoside antibiotics are known to target ribosomal, retroviral and catalytic RNAs with high affinity and specificity. Recently, *in vitro* selection experiments have identified RNA aptamers that bind to aminoglycoside antibiotics with nanomolar affinity and stringent specificity, allowing discrimination between closely related family members. There has, to date, been limited structural information on the molecular basis of such saccharide–RNA recognition.

Results: We describe a solution-structure determination of the tobramycin–RNA aptamer complex, obtained using NMR and molecular dynamics. The structure gives insight into the molecular features associated with saccharide–RNA recognition. Tobramycin adopts a defined alignment and binds to the RNA major groove centered about a stem–loop junction site. A portion of the bound tobramycin is encapsulated between the floor of the major groove and a looped-out cytosine residue that forms a flap over the binding site in the complex.

Conclusions: The emergence of antibiotic-resistant pathogens and their impact on human health continues to be a major concern in the medical community. Rational modification of existing antibiotics aimed at improving their efficacy requires a molecular view of their receptor-binding sites. We have provided such a molecular view for a member of the aminoglycoside antibiotic family that targets RNA.

Address: Cellular Biochemistry and Biophysics Program, Memorial Sloan-Kettering Cancer Center, New York, NY 10021, USA.

Correspondence: Dinshaw J Patel
E-mail: pateld@mskcc.org

Key words: aminoglycoside–RNA recognition, RNA U-turn motif, saccharide targeting the RNA major groove

Received: **18 November 1996**
Revisions requested: **9 December 1996**
Revisions received: **19 December 1996**
Accepted: **23 December 1996**

Electronic identifier: **1074-5521-004-00035**

Chemistry & Biology January 1997, **4**:35–50

Introduction

The mode of action of antimicrobial aminoglycoside antibiotics (reviewed in [1,2]) has been of great interest ever since these antibiotics were shown to be able to block protein synthesis (reviewed in [3,4]). It soon became apparent that aminoglycoside antibiotics target specific sites on RNA, ranging from functional sites on 16S ribosomal RNA [5,6] and catalytic group I intron RNA [7,8], to the rev response element in HIV RNA [9] and the hammerhead ribozyme RNA [10]. There is limited information available that describes, in molecular terms, the principles associated with sequence/structure-specific recognition of RNA binding sites by the aminoglycosidic antibiotics. Recent developments in *in vitro* selection methods have resulted in the identification of RNA sequences that target aminoglycoside antibiotics with high affinity and specificity [11–13]. The aminoglycoside antibiotics include neomycin [13], tobramycin [11], lividomycin and kanamycin [12], and the selected RNA aptamers can discriminate between closely related family members. We have focused on the complex formed between tobramycin [13,14] (Fig. 1a) and its RNA aptamer (Fig. 1b) which has a dissociation constant (K_d) in the nanomolar range [11]. We have undertaken an NMR–molecular dynamics study of the tobramycin–RNA aptamer complex and report below on the structure of the complex in solution. The structure defines the fold of the bulge-containing stem–loop RNA aptamer and tobramycin in the complex and gives insight into the recognition elements responsible for the high affinity sequence/structure specific complex formation.

Results

Complex formation

We followed formation of the tobramycin–RNA aptamer complex by monitoring the imino protons of the RNA aptamer upon gradual addition of tobramycin. The imino proton spectra (8.5–15.5 ppm) of the free RNA aptamer and the 1:1 complex with bound tobramycin in H_2O buffer (10 mM phosphate), pH 6.8 at 5°C are plotted in Figure 2a and 2b, respectively. We detect separate imino proton resonances for the free and bound RNA aptamer at substoichiometric ratios, indicating slow exchange due to the formation of a high affinity complex. Imino proton resonances that are broad in the free RNA aptamer (Fig. 2a) sharpen and shift on formation of the tobramycin–RNA aptamer complex (Fig. 2b).

Exchangeable nucleic acid protons

The exchangeable imino protons have been assigned on the basis of analysis of a series of multinuclear multidimensional NMR experiments on tobramycin complexed to unlabeled and uniformly ^{13}C,^{15}N-labeled RNA aptamers in H_2O buffer solution. These included nuclear Overhauser

Figure 1

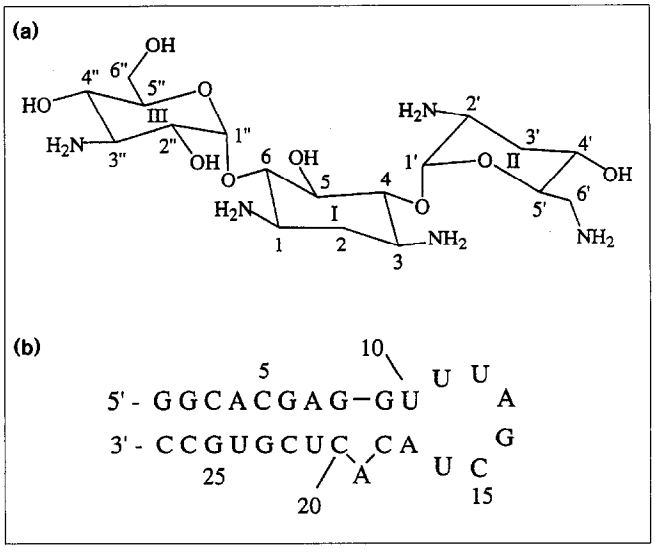

Tobramycin and the 27-nucleotide RNA aptamer. **(a)** Chemical formula and numbering system of tobramycin. The amine protons are positively charged through protonation at pH 6.8. **(b)** Sequence and numbering system of the 27-nucleotide RNA aptamer.

Figure 2

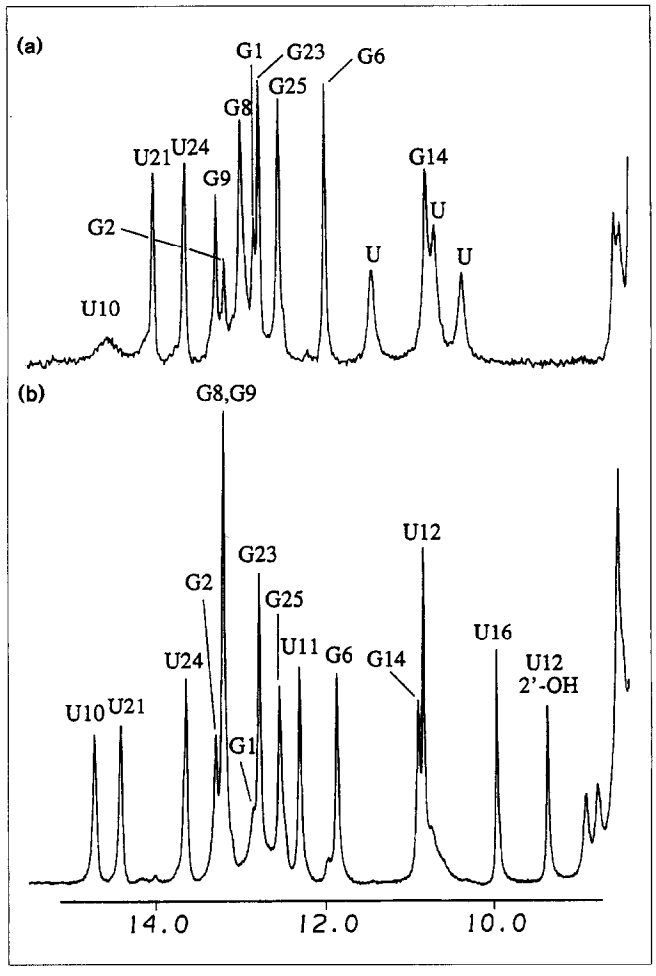

Formation of the tobramycin–RNA aptamer complex. Imino proton NMR spectra (8.5–15.5 ppm) of **(a)** the 27-nucleotide RNA aptamer and **(b)** the tobramycin–RNA aptamer complex in H_2O buffer (10 mM phosphate) at pH 6.8 and 5°C. The imino proton assignments are indicated over the spectra.

effect spectroscopy (NOESY), ^1H–^{15}N heteronuclear single quantum coherence (HSQC), two-dimensional versions of ^1H–^{15}N hetero multiple quantum coherence (HMQC)–NOESY and ^1H–^{13}C HMQC– NOESY and ^1H–^{13}C–^{15}N HCCNH–total correlation spectroscopy (TOCSY) experiments. An expanded NOESY (150 ms mixing time) contour plot of the unlabeled complex outlining NOEs in the symmetrical imino proton region (9.0–15.0 ppm) in H_2O buffer at 0°C is plotted in Figure 3a. We can trace NOEs between imino protons on adjacent base pairs along the stem of the helix and into the hairpin loop (U10–U11–U12 segment) of the RNA aptamer in the complex (Fig. 3a). Unfortunately, the imino protons of G8 and G9 of the G•C base pairs that flank the A19 bulge are superpositioned at 13.20 ppm in the imino proton spectrum of the complex (Fig. 3b).

We made two analogs of the RNA aptamer in which the G8•C20 pair was replaced either by the I8•C20 pair or the A8•U20 pair, and we recorded one- and two-dimensional NMR spectra of these RNA aptamer analog complexes. The imino proton spectra establish that both aptamer analogs form high affinity complexes. The imino proton of I8 of the I8•C20 pair resonates at 15.11 ppm with a somewhat broadened line width, whereas the imino proton of U20 of the A8•U20 pair is too broad to be detectable in the spectra of the complex. This suggests that the base pair at the 8•20 position is less stable than its counterpart at the 9•18 position in the complex, possibly reflecting the contribution of the A19 bulge base that is flanked by these base pairs in the sequence of the RNA aptamer. The imino protons of G8 (13.20 ppm) and G9 (13.28 ppm) are partially resolved when the bulged A19 residue is replaced by its G19 purine counterpart and this substitution has no effect on complex formation as monitored in the imino proton spectral region. The complex can also form when G14 is replaced by A14 and when C15 is replaced by A15, as monitored by the imino proton spectra in the tobramycin–RNA aptamer analog complexes. These studies on the five RNA aptamer analogs which bind tobramycin with the same sequence specificity and similar high affinity confirm the imino proton assignments in the free RNA aptamer and the tobramycin–RNA aptamer complex that are indicated over the resonances in Figure 2a and b, respectively.

The imino protons can also be linked to their attached nitrogens by recording ^1H–^{15}N HSQC spectra on the complex made up of tobramycin and labeled RNA aptamer

Figure 3

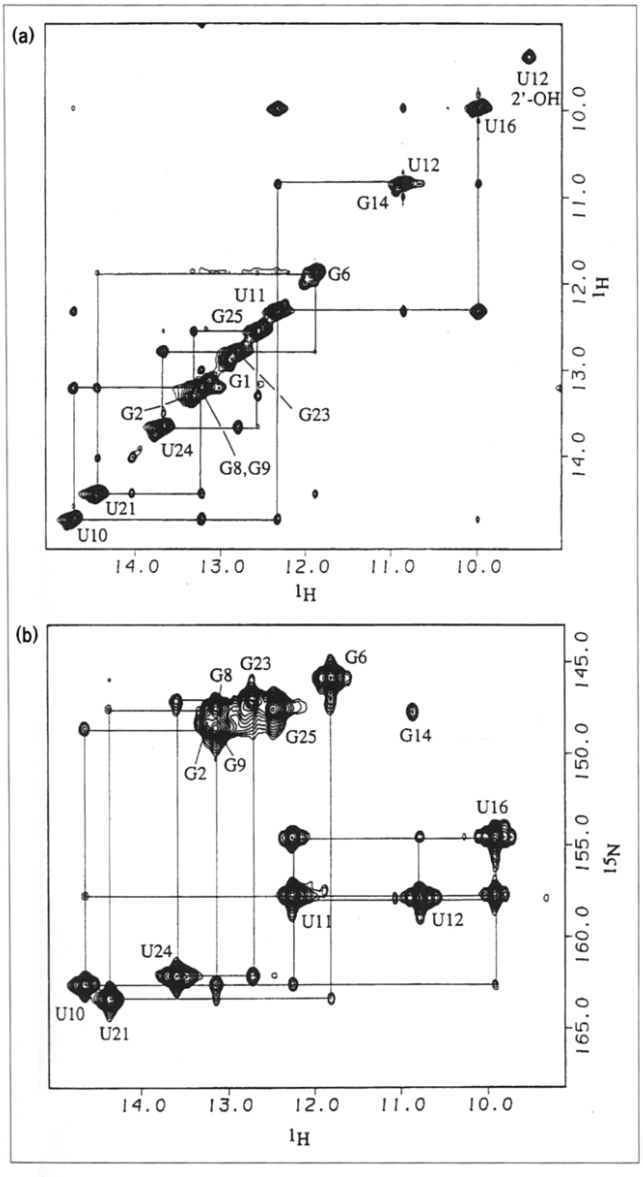

Assignment of exchangeable nucleic acid protons. **(a)** An expanded NOESY (150 ms mixing time) contour plot of the symmetrical imino proton region (9.0–15.0 ppm) of the tobramycin–RNA aptamer complex in H_2O buffer solution, pH 6.8 at 0°C. The lines trace the NOE connectivities between imino protons on adjacent base pairs along the stem segments of the RNA aptamer in the complex. **(b)** An expanded contour plot of a two-dimensional version of the ^{1}H–^{15}N HMQC–NOESY (150 ms mixing time) experiment identifying correlations between imino protons and attached nitrogens in the tobramycin–^{13}C,^{15}N-labeled RNA aptamer complex in H_2O buffer solution, pH 6.8 at 0°C. The lines trace the connectivities between adjacent base pairs along the stem segments of the RNA aptamer in the complex.

in H_2O buffer. The uracil and guanine imino nitrogens have distinct chemical shifts, allowing a straightforward differentiation between the uracil and guanine imino protons in the complex. The two-dimensional version of the ^{1}H–^{15}N HMQC–NOESY experiment permits a sequential walk between imino protons on adjacent base pairs in the stem and adjacent bases in the loop as outlined in the expanded contour plot for the tobramycin–^{13}C,^{15}N-labeled RNA aptamer complex in H_2O buffer at 0°C (Fig. 3b).

Base-pairing alignments

The pairing alignments for stem base pairs — (G1–G8)•(C20–C27) and (G9–U10)•(A17–C18) — can be readily characterized by NOE patterns that monitor connectivities across the base pair in the helix. Watson–Crick alignments are characterized by an NOE between the uracil imino and adenine H2 protons across A•U base pairs and by NOEs between the guanine imino and cytosine amino protons across G•C base pairs in the stem segments. We can readily monitor these patterns within the stem segments for all base pairs in the complexes of tobramycin with the RNA aptamer and its analogs, establishing Watson–Crick alignment along the entire stem of the RNA in the complex. The imino protons of G8 and G9 are resolved in the RNA-aptamer analog, containing a G19 for A19 substitution, and the data establish that the G8•C20 and G9•C18 pairs also form a Watson–Crick alignment. The above analysis was aided by our ability to distinguish between purine H8 and H2 protons by recording a two-dimensional version of the ^{1}H–^{13}C HMQC–NOESY experiment on the tobramycin–^{13}C,^{15}N-labeled RNA aptamer complex, and using the large chemical shift difference between purine C8 and C2 carbons to make the distinction.

RNA sugar 2′-hydroxyl protons

We have also recorded and compared one-dimensional and two-dimensional NOESY spectra with and without broadband ^{13}C and ^{15}N decoupling, to differentiate between RNA protons bound to carbon, nitrogen and oxygen in the tobramycin–^{13}C,^{15}N-labeled RNA aptamer complex in H_2O buffer solution. Such experiments have permitted us to assign the narrow exchangeable proton at 9.36 ppm to a sugar 2′-OH proton that has been assigned to U12 based on its through-space (NOESY) and through-bond (TOCSY) connectivities (to the nonexchangeable sugar protons of U12) in the complex.

Correlation of exchangeable and nonexchangeable nucleic acid protons

NMR methods have been developed recently that permit the through-bond correlation of the exchangeable imino protons with nonexchangeable base protons within individual guanine and uracil rings in RNA and ligand–RNA complexes [15–17]. Expanded plots of the HCCNH–TOCSY experiment outlining through-bond correlations between uracil imino protons and either uracil H5/H6 protons or uracil C6 carbons in the complex are shown in Figure 4a and 4b, respectively. Weaker correlations are also observed between guanine imino protons and H8 protons/ C8 carbons in this experiment (Fig. 4a,b), with these correlations being more clearly detected for

Figure 4

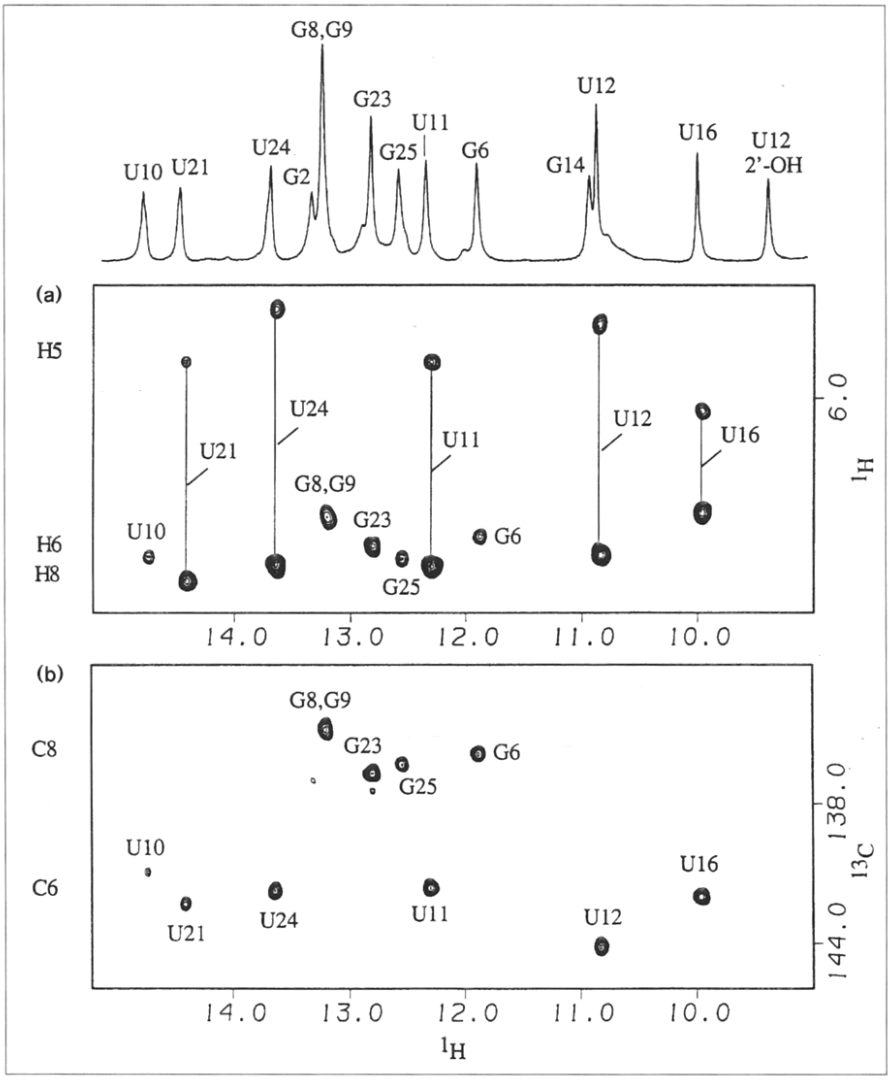

Through-bond correlation between exchangeable and nonexchangeable nucleic acid protons. Expanded contour plots of HCCNH–TOCSY experiments on the tobramycin–^{13}C,^{15}N-labeled RNA aptamer complex in H_2O buffer solution, pH 6.8 at 10°C. These experiments were optimized for the uracil imino proton region and correlate uracil imino protons with **(a)** their own H5 and H6 protons and **(b)** C6 carbons. Weaker cross peaks are also observed for correlations between the guanine imino protons and (a) their own H8 protons or (b) C8 carbons. The following changes were made in the HCCNH–TOCSY experiment to optimize for uracil relative to our previous optimization for guanine [15]: the ^{13}C frequency was set to 137 ppm; the ^{13}C TOCSY transfer was achieved by a DIPSI-3 spin lock applied at a power of 9.5 kHz for 17 ms; a 650 ms REBURP pulse was used as the selection pulse on ^{13}C; a constant time version of the experiment was used for the ^{1}H–^{13}C correlation with a 15 ms constant time evolution period on carbon.

HCCNH–TOCSY experiments optimized for guanine imino protons in the complex. The through-bond correlations between exchangeable and nonexchangeable protons within individual uracils and guanines are essential for linking exchangeable and nonexchangeable proton assignments in the complex.

Nonexchangeable nucleic acid protons

The nonexchangeable base and sugar protons of the tobramycin–RNA aptamer complex have been assigned following analysis of multinuclear multidimensional (NOESY, COSY, TOCSY, ^{1}H–^{13}C NOESY–HMQC and ^{1}H–^{13}C HCCH–COSY and HCCH–TOCSY) data sets in D_2O solution. The NOE cross-peaks are reasonably well resolved in expanded NOESY contour plots, correlating the base protons with their own and 5′-flanking sugar H1′ protons in the complex in D_2O buffer, at pH 6.8 and 25°C. These connectivities are traced for the A7–U21 segment in Figure 5a, with the connectivities either weak or absent at the U12–A13, G14–C15 and C18–A19 steps, indicating structural discontinuities at these steps in the complex.

The connectivities can be independently assigned with additional confidence following dispersion of the two-dimensional data into a third heteronuclear dimension according to the chemical shifts of the attached carbons. This has been achieved by analyzing the ^{1}H–^{13}C NOESY–HMQC spectra of the tobramycin–^{13}C,^{15}N-labeled RNA aptamer complex in D_2O buffer at 25°C, as shown in strip plots illustrating sequential connectivities from A7 to U21 in Figure 5b. We also note weak or absent connectivities at the U12–A13, G14–C15 and C18–A19 steps in this data set, as well as connectivities between non-adjacent U12 and G14 residues and between non-adjacent G14 and G16 residues in the complex (Fig. 5b). The H8 proton of A19 has an unusual downfield shift of

Figure 5

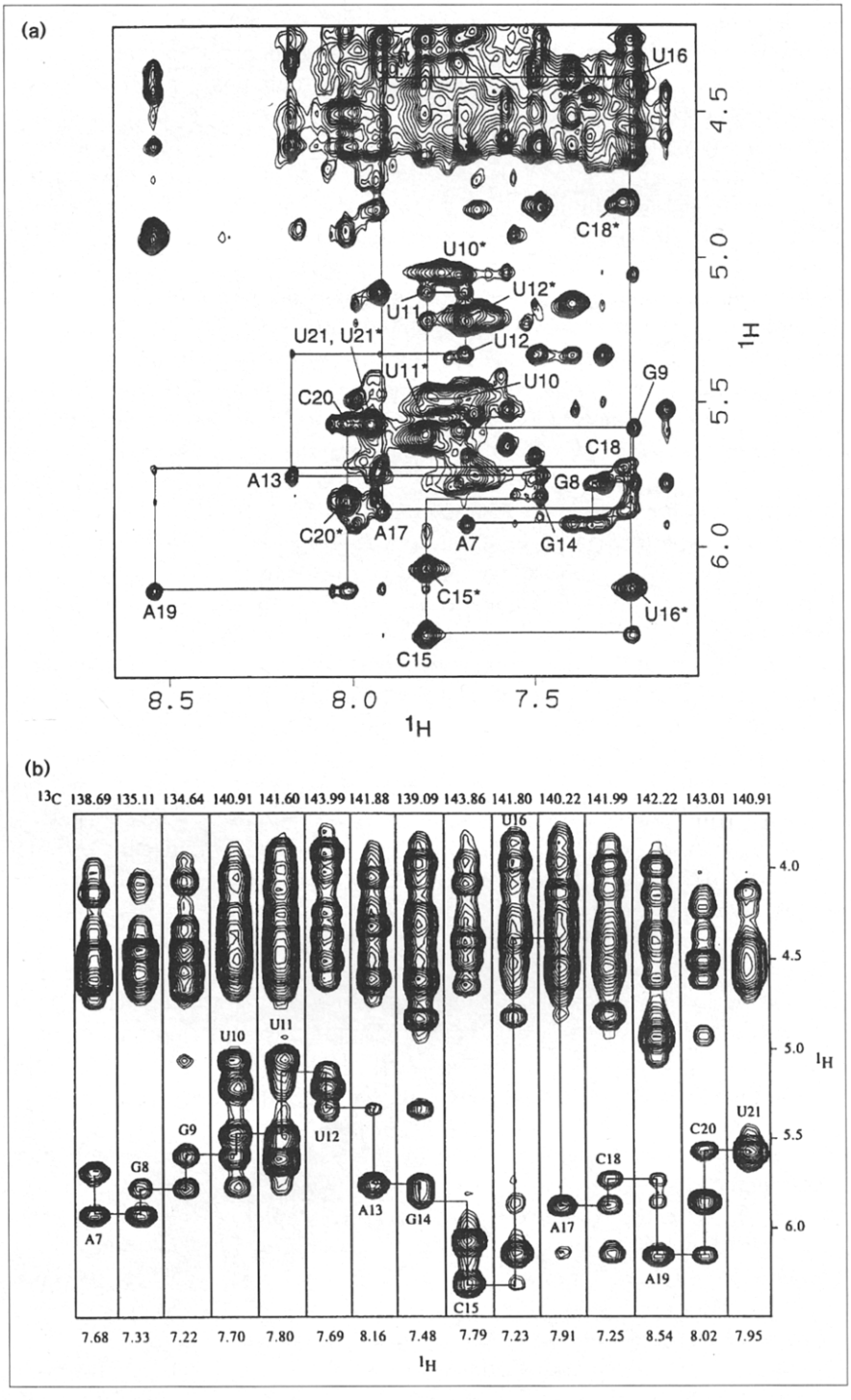

Figure 5

Assignment of nonexchangeable nucleic acid protons. **(a)** An expanded NOESY (300 ms mixing time) contour plot identifying NOEs between the base protons (7.0–8.6 ppm) and the sugar H1′ protons (4.3–6.5 ppm) of the tobramycin–RNA aptamer complex in D_2O buffer, pH 6.8 at 25°C. The lines trace the NOE connectivities between the base and its own and 5′-flanking sugar H1′ protons for the A7 to U21 segment. The strong H5–H6 NOE cross-peaks of the uracils and the cytosines are designated by asterisks. **(b)** A plot of two dimensional ^{1}H–^{1}H spectral strips at specific purine C8/pyrimidine C6 carbon chemical shift values taken from the three-dimensional ^{1}H–^{13}C NOESY-HMQC (300 ms mixing time) experiment on the tobramycin–^{13}C,^{15}N-labeled RNA aptamer complex in D_2O buffer solution, pH 6.8 at 25°C. The lines trace NOE connectivities between base protons and their own and 5′-flanking sugar H1′ protons from A7–U21.

8.54 ppm, the H5 proton of C15 has an unusual downfield shift of 6.07 ppm and the H1′ proton of U16 has an unusual upfield shift of 4.38 ppm in the proton spectra of the complex. Furthermore, we observe a strong NOE between the H6 and H1′ protons of C15 in a short mixing-time NOESY data set [18] for this residue in the complex.

These data provide a complete set of base and sugar H1′ proton assignments in the tobramycin–RNA aptamer complex. The remaining sugar protons can be linked through coupling connectivities starting from the sugar H1′ protons in ^{1}H–^{13}C HCCH–COSY and HCCH–TOCSY experiments resulting in the assignment of the majority of

the nonexchangeable sugar proton and attached carbon chemical shifts in the tobramycin–^{13}C,^{15}N-labeled RNA aptamer complex at 25°C. Furthermore, the H8 and H2 nonexchangeable base protons of individual adenine residues have been linked as the result of a two-dimensional version of the ^{1}H–^{13}C HCCH–TOCSY experiment on the complex at 25°C.

We have monitored through-bond proton connectivities between sugar H1′ and H2′ protons to qualitatively distinguish between C2′-endo (large coupling constant) and C3′-endo (negligible coupling constant) families of sugar pucker geometries in the tobramycin–RNA aptamer complex. We observe strong H1′–H2′ cross-peaks for C15 and A19, implying sugar puckers in the C2′-endo range for these residues in the complex. In addition, weak coupling cross-peaks are observed for the A17 and C18 residues in the complex.

Cross-strand interactions in the RNA hairpin loop

A set of cross-strand NOEs are observed within the U11–U12–A13–G14–C15–U16 segment of the hairpin loop in the tobramycin–RNA aptamer complex. A strong NOE is observed between the imino protons of U11 and U16 and a weaker NOE observed between the imino protons of U12 and U16 across the RNA hairpin loop in the complex (Fig. 3a). In addition, cross-strand NOEs are observed between the protons of U12 and G14, including one between the 2′-OH of U12 and the H8 proton of G14 and another between the H1′ proton of U12 and the H8 proton of G14 (Fig. 5a) in the complex. These cross-strand NOEs provide critical restraints for defining the conformation of the hairpin loop in the complex.

Phosphate backbone

We observe several phosphorus resonances shifted outside the –3.8 to –4.7 ppm range, characteristic of unperturbed backbone phosphates in the proton-decoupled phosphorus NMR spectrum of the tobramycin–RNA aptamer complex in D_2O buffer at 25°C. These phosphorus resonances have been assigned on the basis of analysis of proton-detected multinuclear multidimensional (^{1}H–^{31}P and ^{1}H–^{13}C–^{31}P) correlation experiments on the complex. Large downfield phosphorus chemical shifts are observed at the A13–G14 (–2.59 ppm), A19–C20 (–2.36 ppm) and U12–A13 (–1.40 ppm) steps, whereas a large upfield shift is observed at the G14–C15 (–6.05 ppm) step, suggesting there are conformational perturbations in the backbone for the U12–A13–G14–C15 segment of the hairpin loop and the A19–C20 step at the bulge site in the complex.

Tobramycin protons

Tobramycin consists of a central non-sugar ring, deoxystreptamine (labeled I in Fig. 1a), attached through glycosidic linkages in either direction to amino sugars, 2-amino-3-deoxy-6-aminoglucose and 3-aminoglucose (labeled II and III, respectively, in Figure 1a). The proton NMR spectra of free tobramycin have been recorded and analyzed in aqueous solution [19], and crystal structures are available for the related aminoglycoside antibiotic kanamycin both in the free state [20] and when bound to kanamycin nucleotidyltransferase [21].

We have differentiated between the protons of rings I, II and III of tobramycin (Fig. 1a) in its complex with the RNA aptamer. Rings II and III are amino sugars and hence distinct from non-sugar ring I in the tobramycin molecule. Furthermore, ring II contains methylene protons at position 3′ (Fig. 1a), while ring III lacks methylene protons making it possible to differentiate between tobramycin rings II and III on the basis of their patterns of through-bond and through-space connectivities in the complex. The NOE connectivities from the H1′ proton of ring II and the H1″ proton of ring III are outlined in the NOESY (300 ms mixing time) contour plot of the tobramycin–RNA aptamer complex in D_2O buffer at 25°C in Figure 6a, and these patterns have been confirmed using the corresponding ^{13}C-filtered NOESY data on the tobramycin–^{13}C,^{15}N-labeled RNA aptamer complex.

The H4 and H6 protons of tobramycin non-sugar ring I are in similar chemical environments and have been assigned based on NOEs between the H1′ proton of ring II and the H4 proton (and to a lesser extent H6 proton) of ring I, and between the H1″ proton of ring III and the H6 proton (and to a lesser extent H4 proton) of ring I in NOESY spectra, recorded as a function of mixing time on the complex. The H1 and H3 protons of tobramycin ring I are also in similar chemical environments and are separated by methylene protons at position 2 (Fig. 1b). These tobramycin non-sugar ring I protons exhibit resolved chemical shifts for the H4 (4.01 ppm) and H6 (3.81 ppm) protons and resolved chemical shifts for the H1 (3.78 ppm) and H3 (3.93 ppm) protons in the complex.

A few tobramycin exchangeable protons can be observed and assigned in the NMR spectrum of the complex on the basis of NOE and coupling connectivities to adjacent nonexchangeable protons. These include the 2′-NH_3^+ (7.40 ppm) proton on ring II, the 1-NH_3^+ (8.11 ppm) and 5-OH (7.03 ppm) protons on ring I and the 4″-OH (7.19 ppm) and 6″-OH (7.58 ppm) protons on ring III in the complex (Fig. 6b).

Intermolecular NOEs in the complex

We have identified 34 intermolecular NOEs between tobramycin and the RNA aptamer in the complex (Table 1). The observed degeneracy in several of the tobramycin proton chemical shifts complicated the assignment of intermolecular NOEs in the complex. Thus, the H6 proton on ring I and the H2″ proton on ring III exhibit the same chemical shift of 3.81 ppm in the complex. The intermolecular NOE between the 3.81 ppm resonance and the

Figure 6

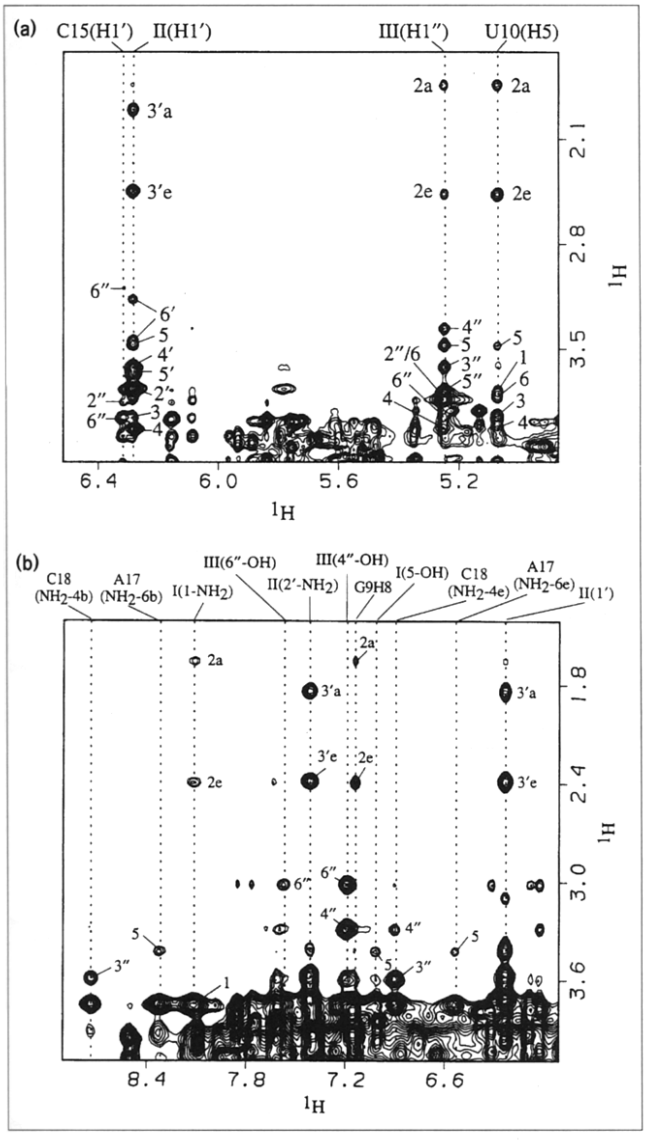

Assignment of tobramycin exchangeable and nonexchangeable protons. **(a)** An expanded NOESY (300 ms mixing time) contour plot correlating NOEs between the 4.9–6.5 ppm region and the 1.6–4.4 ppm region of the tobramycin–RNA aptamer complex in D_2O buffer solution, pH 6.8 at 25°C. This plot outlines NOEs originating in the tobramycin amino sugar ring II anomeric H1′ proton and amino sugar ring III anomeric H1″ proton, as well as NOEs originating in the RNA C15(H1′) and U10(H5) protons in the complex. The cross-peaks are labeled by their tobramycin nonexchangeable proton assignments in the complex. **(b)** An expanded NOESY (200 ms mixing time) contour plot correlating NOEs between the 5.8–9.0 ppm region and the 1.4–4.0 ppm region of the tobramycin–RNA aptamer complex in H_2O buffer solution, pH 6.8 at 5°C. This plot outlines NOEs originating in the tobramycin and RNA exchangeable protons in the complex. The cross-peaks are labeled by their tobramycin nonexchangeable proton assignments in the complex.

H5 proton of U10 is tentatively assigned to an NOE between ring-I(H6) and U10(H5), because an unambiguous

Table 1

Intermolecular NOEs between tobramycin and RNA aptamer protons in the complex.

Tobramycin	Chemical shifts	RNA
ring I		
H1	3.78 ppm	U10(H5)
H2a	1.71 ppm	U10(H5), G9(H8)
H3	3.93 ppm	U10(H5)
H4	4.01 ppm	U10(H5)
H5	3.45 ppm	U10(NH3,H5), U11(NH3), A17(NH_2-6b, e)
H6	3.81 ppm	U10(H5)
ring II		
H2′	3.74 ppm	U12(NH3)
2′-NH_2	7.40 ppm	U11(NH3), U12(NH3)
H3′a	1.56 ppm	U12(NH3)
ring III		
H1″	5.23 ppm	C15(H5)
H2″	3.81 ppm	C15(H5, H1′)
H3″	3.60 ppm	A19(H2), C18(NH_2-4b, e)
H4″	3.33 ppm	C15(H5, H6), C18(NH_2-4e)
4″-OH	7.19 ppm	C18(NH_2-4b, e)
H5″	3.76 ppm	C15(H5)
H6″	3.94 ppm	C15(H5, H1′)
H6″	3.06 ppm	C15(H5, H6, H1′)
6″-OH	7.58 ppm	A17(NH_2-6b, e)

NOE was also observed between ring-I(H5) and U10(H5) in the complex (Table 1).

Tobramycin amino sugar ring III exhibits the most intermolecular NOEs, whereas amino sugar ring II exhibits the least intermolecular NOEs in the tobramycin–RNA aptamer complex (Table 1). Significantly, protons on ring III exhibit many intermolecular NOEs to the base (H5 and H6) and sugar (H1′) protons of C15 in the complex. The majority of the intermolecular NOEs involving non-sugar ring I protons are to the base H5 proton of U10 in the complex. The only assignable intermolecular NOEs involving protons on ring II are to the imino protons of U11 and U12 in the complex.

Input restraints

Inter-proton distance restraints were quantified from NOE buildup curves in NOESY experiments on the tobramycin–RNA aptamer complex in H_2O (two mixing times) and D_2O (four mixing times) buffer solutions. Additional distance restraints were obtained from analysis of a three-dimensional NOESY–HMQC spectrum recorded at a single mixing time on the complex. Hydrogen-bond restraints were incorporated for the Watson–Crick base pairs in the helical stem of the RNA in the complex. Torsion-angle restraints were imposed on selected ribose sugars to maintain appropriate puckers. Additional details on the restraints sets and bounds are described in the Materials and methods section. The input-restraint

statistics and their partitioning into several categories for the tobramycin–RNA aptamer complex are summarized in Table 2.

Structure calculations

The refinement strategy used to define the solution structures of the tobramycin–RNA aptamer complex is outlined briefly below and in more detail in the Materials and methods section. The initial starting structures of the RNA aptamer contained A-form stem segments and stacked bulge and hairpin-loop residues. Tobramycin was next positioned at the center of mass of the RNA duplex in a randomized orientation. The molecular dynamics calculations were performed at 1000K on the entire complex, initially with the intermolecular nonbonded interactions between tobramycin and RNA turned off, and subsequently with the full potential energy function turned on during the computations. Seven low-energy distance-refined solution structures of the tobramycin binding domain (residues 7–21) of the RNA aptamer are shown in stereo in Figure 7a while a representative structure of the complex is shown in stereo in Figure 7b.

Structure analysis

The superpositioned distance-refined structures of the tobramycin–RNA aptamer complex (Fig. 7a) exhibit low total energy, low root mean square (rms) deviation energy gradients and a low van der Waals energy while satisfying the NOE-derived distance restraints (Table 2). The tobramycin binds in the major groove of the RNA aptamer spanning residues G9–U12 and G14–C18 which are centered about the stem–hairpin-loop junction in the complex (Fig. 7b). The bulged A19 base (Fig. 8b) and the looped out C15 residue (Fig. 8a) are important components of the RNA-binding pocket in the tobramycin complex.

The penetration of the tobramycin molecule into the major groove of the RNA aptamer, together with the role of the C15 base as a flap, are highlighted in views of the complex shown in Figure 9a and b. Tobramycin ring III, and to a lesser extent ring I, are sandwiched between the floor of the major groove and the C15 base flap, while ring II interacts less intimately (Fig. 9c) with the major groove of the RNA aptamer in the complex. The intermolecular interactions of tobramycin rings III and I with the floor of the major groove in the complex are shown in Figure 8c and 8d. The relative orientations of the positively charged NH_3^+ groups on the tobramycin and the backbone phosphates on the RNA aptamer in the complex viewed down the major groove are shown in Figure 9d.

The hairpin-loop spanning residues U11–U12–A13–G14–C15–U16 of the RNA aptamer adopt a specific folded conformation on formation of the complex with tobramycin. The fold of the U12–A13–G14 segment is stabilized by a pair of cross-strand hydrogen bonds (Fig. 10a), as well as stacking of A13 and G14 purine residues in the complex (Fig. 10d). The hairpin-loop U11 and U16 bases align through formation of a pair of Wobble hydrogen bonds (Fig. 10c) and extend the stem by an additional U•U mismatch pair in the complex.

Table 2

Statistics of NMR data of the seven refined structures of the tobramycin–RNA aptamer complex.

NMR distance restraints		495
RNA aptamer		416
Intra-residue	149	
Sequential (|i–j| = 1)	144	
Long range (|i–j| ≥ 2)	123	
Hydrogen bond	54	
Tobramycin		45
Tobramycin–RNA aptamer		34
Structure statistics		
NOE violations		
Number > 0.1 Å		1–2
Number > 0.2 Å		0
rms deviations of violations (Å)		0.014 ± 0.001
Deviations from ideal covalent geometry		
Bond length (Å)		0.008 ± 0.001
Bond angle (°)		2.941 ± 0.317
Impropers (°)		0.417 ± 0.020
Pairwise rms deviation (Å) amongst the seven refined structures		
RNA aptamer		
Residues A7–U21 (excluding C15)		1.98 ± 0.51
Residues G9–C18 (excluding C15)		1.13 ± 0.18
Tobramycin		
Residues I, II and III		0.80 ± 0.28
Tobramycin–RNA aptamer complex		
Tobramycin (I, II and III) and RNA residues A7–U21 (excluding C15)		2.00 ± 0.46
Tobramycin (I, II and III) and RNA residues G9–C18 (excluding C15)		1.24 ± 0.20

The most striking feature of the tobramycin–RNA aptamer complex is that the aminoglycoside antibiotic is partially encapsulated within a channel generated between the floor of the major groove and the pyrimidine ring of C15 at the binding site. Surface representations of the channel and its partially encapsulated tobramycin are shown in views looking into the major groove in Figure 11a and 11c and looking into the minor groove in Figure 11b and 11d.

Discussion

The present study of tobramycin has focused on its complex with an RNA aptamer rather than the natural ribosomal RNA target because the binding is much tighter to the RNA aptamer (nanomolar) than to the ribosomal RNA target (millimolar). The decision to work on the RNA aptamer with its high-affinity binding for tobramycin accounts for the excellent quality of the NMR spectra observed for the complex. Previous research identified two RNA aptamers that bound to tobramycin with

Figure 7

Structure of the core of the tobramycin–RNA aptamer complex. **(a)** A stereo view of seven superimposed distance-refined structures of the extended core (residues A7–U21 and tobramycin) of the tobramycin–RNA aptamer complex. The RNA bases are colored blue except for residues C15 and A19 which are pink, the RNA backbone is orange and the bound tobramycin is greeny yellow. The superposition was performed on all heavy atoms of tobramycin and G9–C18 RNA residues excluding C15. **(b)** A stereo view of one representative refined structure of the core (residues A7–U21 and tobramycin) of the tobramycin–RNA aptamer complex.

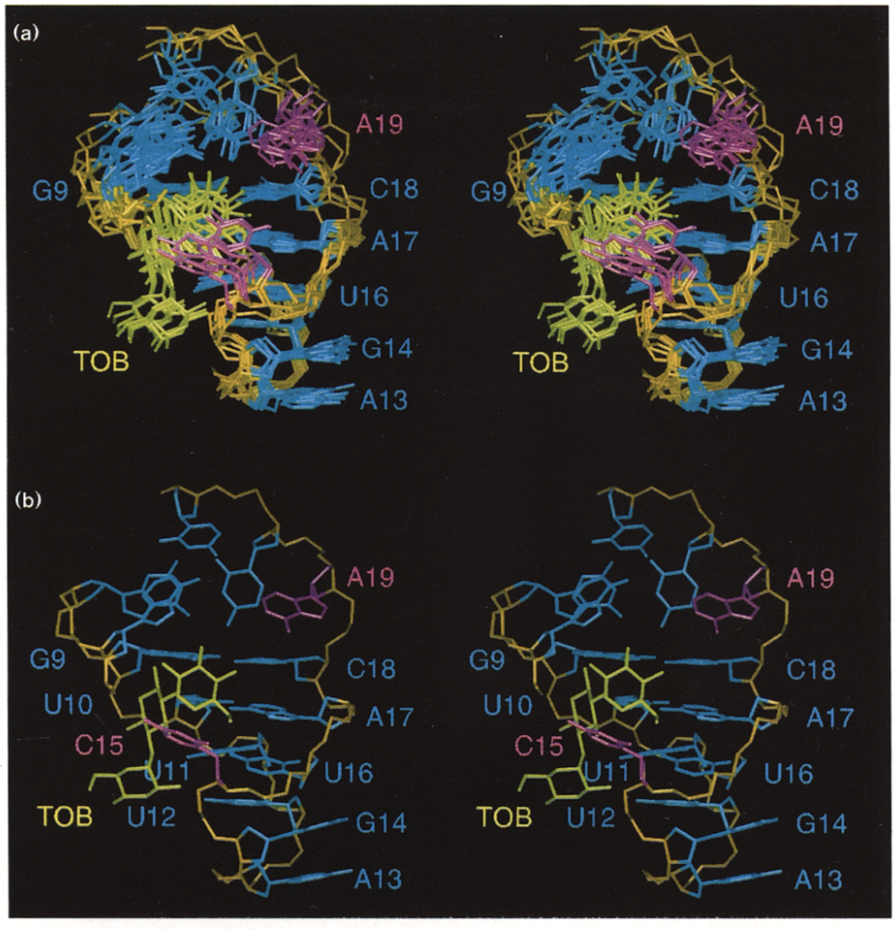

nanomolar affinity [11]. The present study reports on the solution structure of the complex between one such RNA aptamer and tobramycin, and efforts are currently under way to solve the structure of the other tobramycin–RNA aptamer complex.

Spectral quality

We have obtained very high quality NMR spectra for the tobramycin–RNA aptamer complex as exemplified by the narrow and well-resolved imino proton resonances of the complex recorded in Figure 2b. The quality of the spectra reflect complex formation involving binding of tobramycin with sequence and structural specificity and with high affinity at a single site on the RNA aptamer. The application of multinuclear multidimensional NMR methods to the tobramycin–uniformly ^{13}C,^{15}N-labeled RNA-aptamer complex readily yielded the RNA assignments in the complex. We do not have access to isotopically labeled tobramycin so the aminoglycoside antibiotic assignments in the complex were deduced from standard and ^{13}C-filtered NMR experiments. Such an approach yielded all the nonexchangeable and a few exchangeable proton (NH_3^+ and OH) assignments of tobramycin in the complex. The major limitation was the near degeneracy in the chemical shifts of several tobramycin nonexchangeable protons that restricted somewhat the number of intermolecular NOEs that could be unambiguously assigned and used in the structure calculations for the complex.

Quality of the refined structures

We have used a robust computational protocol in our efforts to define the solution structure of the tobramycin–RNA aptamer complex. There was no bias in the alignment of the tobramycin molecules, because they were positioned in a randomized orientation at the center of mass of the initial RNA conformation at the start of the distance-restrained molecular dynamics calculations. This approach placed the tobramycin molecules in a randomized orientation at the (G6–G8)•(C20–C22) segment at the start of the calculations and resulted in a defined orientation at (G9–U12)•(C15–C18) segment at the end of the calculations. We also insured that there was no bias in the choice of starting conformations within the tobramycin-binding G9–A19 segment of the RNA aptamer in the early stages of the molecular dynamics calculations. Thus, Watson–Crick base pairing was enforced only for the (G1–G8)•(C20–C27)

Figure 8

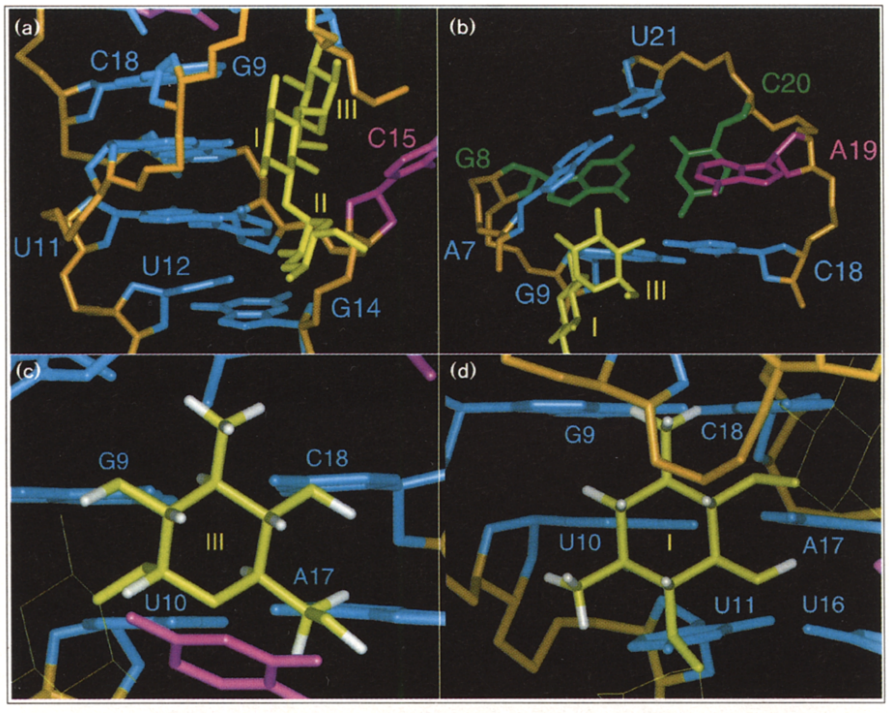

Intermolecular interaction between tobramycin and RNA. **(a)** The alignment of tobramycin (in greeny yellow) within the major groove of the (G9–U10–U11–U12)•(G14–C15–U16–A17–C18) segment in one representative refined structure of the tobramycin–RNA aptamer complex. **(b)** A view of (A7–G8–G9)•(C18–A19–C20– U21) and rings I and III of tobramycin in one representative refined structure of the tobramycin–RNA aptamer complex. This view emphasizes the positioning of the bulged A19 base (in pink) relative to its flanking G•C base pairs in the complex. Note that the G8•C20 base is propeller-twisted relative to the G9•C18 base pair in the complex. Views of **(c)** tobramycin amino sugar ring III and **(d)** tobramycin nonsugar ring I in face-down alignments within the major groove of the RNA aptamer helix in one representative refined structure of the complex.

RNA helical segment at the start of the computations and Watson–Crick pairing for the (G9–U10)•(A17–C18) segment was gradually introduced later in the calculations. Snapshots taken at early stages during the trajectory of the molecular dynamics calculations at 1000K established that the G9–A19 segment of the RNA aptamer adequately sampled conformational space. Finally, no hydrogen-bonding restraints were used to restrict the conformation of the U11–U16 hairpin loop and no intermolecular hydrogen-bonding restraints were used to restrict the alignment of the tobramycin on the RNA aptamer.

The conformation of tobramycin in the complex is well defined since we observe rms deviation values of 0.80 Å±0.28 (Table 2) following superposition of only the aminoglycoside antibiotics within the seven distance-refined structures of the complex. Similarly, the G9–C18 segment (excluding the looped-out C15 residue) is well defined, because we observe rms deviation values of 1.13 Å±0.18 (Table 2) following superposition of only this RNA segment within the seven distance-refined structures of the complex. The finite number of unambiguous intermolecular restraints, however, results in a small spread in the alignment of the tobramycin within the RNA major groove of the complex (Fig. 6a).

The seven distance-refined structures of the tobramycin–RNA aptamer complex (entire tobramycin and RNA residues A7–U21 excluding C15) exhibit rms deviation values in the range 2.0 Å±0.46 (Table 2). There is a spread in the position of the A19 bulged base amongst the refined structures (Fig. 6a), which in turn affects the orientation of the long helix with respect to the tobramycin-binding site. Thus, the rms deviation values reduce to 1.24 Å±0.20 (Table 2) for the core of the complex (entire tobramycin and RNA residues G9–C18 excluding C15).

Global features of the complex

The tobramycin molecule binds in a defined orientation within the major groove spanning the hairpin-loop–stem junction of the RNA aptamer (Fig. 7b). The RNA binding site spans a mixture of Watson–Crick (G9•C18 and U10•A17) and mismatch (U11•U16) base pairs with the looped out C15 residue being important in the partial encapsulation of the bound tobramycin. The tobramycin targets the RNA major groove such that amino sugar ring II is directed towards the hairpin loop while amino sugar ring III is directed towards the A19 bulged base in the complex (Fig. 8a). The C15 base is looped out of the helix but orients itself as a flap over the tobramycin ring III in the complex (Fig. 8a). The A19 bulged base is displaced partially into the major groove and perturbs stacking between Watson–Crick aligned G9•C18 and G8•C20 base pairs in the complex (Fig. 8b).

Tobramycin alignment in the complex

The conformation of tobramycin in the refined structures of the complex is defined by the torsion angles about

Figure 9

Tobramycin alignment in the major groove of the RNA aptamer. Views **(a)** looking into the major groove and **(b)** looking down the major groove of one representative refined structure of the extended core (residues G6–C22 and tobramycin) of the tobramycin–RNA aptamer complex. These views highlight the positioning of tobramycin (in yellow) in a space-filling representation within the major groove of the RNA backbone (in orange) together with the looped out C15 residue (in pink). **(c)** A GRASP view of the tobramycin molecule in yellow inserted into the RNA major-groove binding pocket closed by the flap-like alignment of the C15 base in one representative refined structure of the complex. **(d)** A view emphasizing the relative positioning of the NH_3^+ groups on the tobramycin (meshed surfaces in blue) and RNA backbone phosphates (meshed surfaces in pink) in one representative refined structure of the complex.

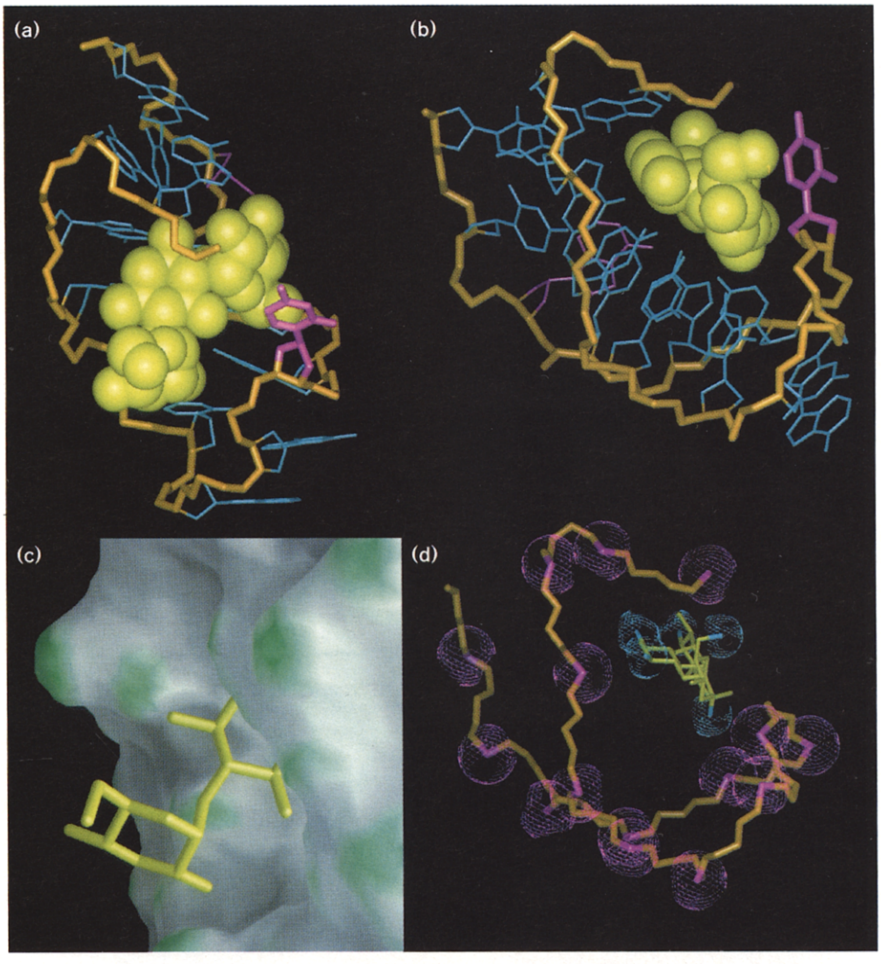

Figure 10

Conformation of the U-turn motif of the RNA aptamer on formation of the complex. A comparision of the RNA fold of **(a)** the U12–A13–G14 turn in one representative refined structure of the tobramycin–RNA aptamer complex with **(b)** the corresponding fold in the three-nucleotide turn of the anticodon loop in the crystal structure of yeast $tRNA^{phe}$. The emphasis is on the hydrogen bond between the 2′-OH of U12 and the N7 of G14 across the loop and the potential hydrogen bond between the imino proton of U12 and the backbone phosphate at the G14–C15 step across the loop in the tobramycin–RNA aptamer complex and its counterpart in the crystal structure of yeast $tRNA^{phe}$. **(c)** The pairing alignment of the U11•U16 mismatch pair in one representative refined structure of the complex. **(d)** Stacking alignment between bases in the U12–A13–G14 segment at the tip of the hairpin loop in one representative refined structure of the complex.

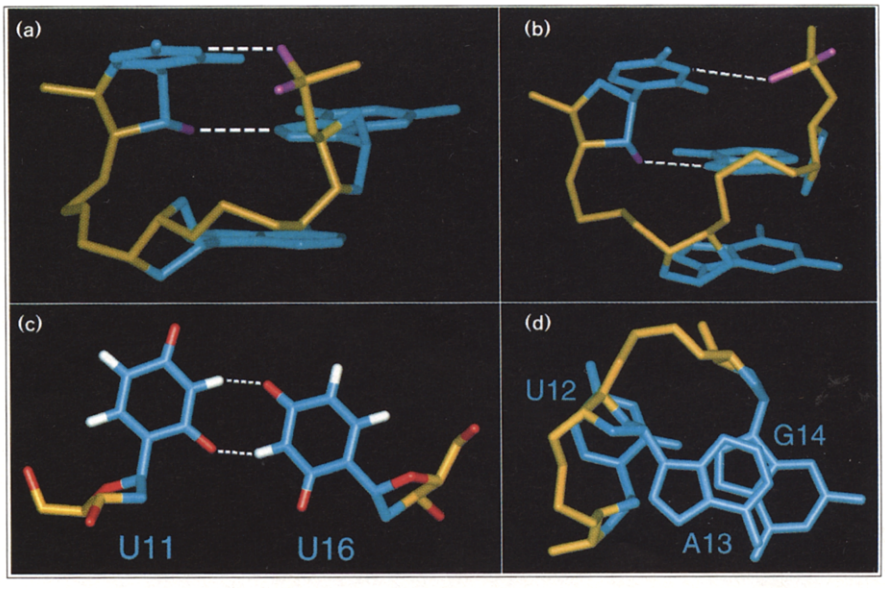

Figure 11

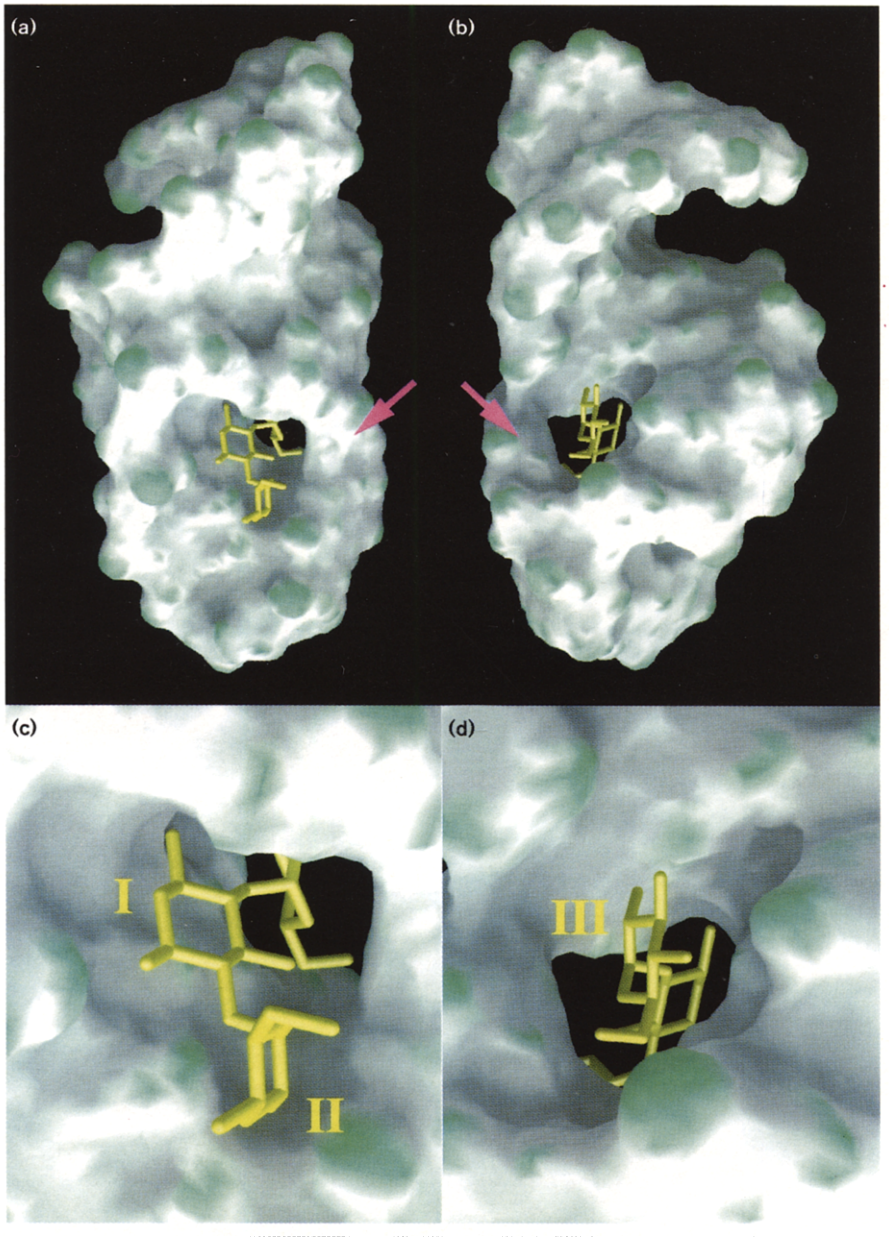

Surface views of one representative refined structure of the tobramycin–RNA aptamer complex. The RNA surface representation is displayed with GRASP33 [43]. Convex and concave surfaces are shown in green and grey, respectively. The bound tobramycin is shown in a stick representation in yellow. The pink arrow points to the C15 base which acts as a flap to close the binding site. **(a)** View of the binding-site channel and its occupancy looking into the major groove of the complex. **(b)** View of the binding-site channel and its occupancy looking into the minor groove of the complex. Views **(c)** and **(d)** are blow ups of the binding site derived from (a) and (b), respectively. The tobramycin rings are labeled I, II and III.

the two glycosidic bonds linking rings III and I and linking rings I and II (Fig. 1a). The III–I linkage is defined by the torsion angles III(H1″)–III (C1″)–O–I (C6) = –7.8° ± 12.1 and III(C1″)–O–I(C6)–I (H6) = 36.9° ± 4.7, whereas the I–II linkage is defined by the torsion angles I(H4)–I (C4)–O–II(C1′) = –34.8° ± 3.6 and I(C4)–O–II(C1′)–II(H1′) = –27.7° ± 17.6 amongst the refined structures of the complex. This narrow distribution implies that the glycosidic linkages between rings of tobramycin are well defined in the refined structures of the complex.

All three tobramycin rings adopt a chair conformation with rings III and I interacting with the RNA major groove in the complex to a greater extent than does ring II. The amino sugar ring of III interacts with the major groove centered about the G9•C18 and U10•A17 base pairs in one representative refined structure of the complex (Fig. 8c). The H3″ and H5″ protons in axial positions and the 2″-OH and 4″-OH hydroxyl groups in equatorial positions along with the 6″-OH hydroxyl on ring III are directed towards the floor of the major groove, while the H2″ and H4″ protons in axial orientations on ring III are directed outwards towards the C15-residue flap that encapsulates the binding site (Fig. 8c). The non-sugar ring I interacts face-down with the major groove, spanning three base pairs centered about the U10•A17 base pair in

one representative refined structure of the complex (Fig. 8d). The H1, H3 and H5 protons in axial orientations on ring I are directed towards the floor of the major groove, while the NH_3^+ groups at the equatorial 1 (8.11 ppm) and 3 positions are aligned approximately parallel to the floor of the groove (Fig. 8d). The amino sugar ring of II lies partially in the major groove with its 2′-NH_3^+ group directed towards the groove.

We have measured the buried surface area of tobramycin and observe that, amongst the distance-refined structures, 51.8% of its surface is buried (203.0 Å^2±26.2 out of a total of 391.7 Å^2±9.7) on complex formation. The buried surface area is asymmetrically distributed amongst the three rings of tobramycin because sugar ring II is the least buried (Fig. 9c) in the complex. Tobramycin was covalently linked to the affinity-chromatography column during *in vitro* selection through the 6′ position of ring II [11] and this linkage may account for the exposure of the 6′ edge of ring II to solvent in the complex.

RNA binding pocket

The binding pocket for tobramycin in the RNA major groove involves elements of both the stem and hairpin-loop segments, and, indirectly, the adenine bulge of the RNA aptamer. The key elements that define the binding pocket include the dimensions of the major groove and the base-pair edges spanning the G9–U12 and G14–C18 segments of the RNA, as well as the orientations of the looped-out C15 base and the bulged A19 base in the complex.

The looped-out C15 residue is important because it contributes to the encapsulation of amino sugar ring III and, to some extent, non-sugar ring I of tobramycin in the complex. Many intermolecular NOEs are observed between protons of C15 and protons on ring III of tobramycin in the complex (Table 1). The downfield chemical shift of the H5 proton of C15 (6.07 ppm) is consistent with the looping of this base out of the helix in the complex. The cytosine H6 and H1′ protons exhibit a separation of 3.12 Å±0.02 amongst the seven refined structures of the complex, which may partially explain the observation of a strong NOE between this pair of protons in the NOESY spectrum of the complex. The C15 residue can be replaced by adenine without affecting the specificity and high affinity of complex formation.

The orientation of the adenine base of the bulged A19 residue is intermediate between stacked-in and looped-out conformations in the refined structures of the complex (Figs 7a and 8b). The H8 proton of A19 is not stacked with flanking bases, which accounts for its downfield chemical shift position of 8.54 ppm in the complex. There is a spread in the relative alignments of the A19 residue and this in turn affects the relative orientation of the two stem segments that flank it in the complex. Amongst the distance-refined structures of the complex, the G9•C18 base pair in one direction shows minimal propeller twist (−1.4°±11.3), while a larger propeller twist (10.5°±36.8) is observed for the G8•C20 base pair in the other direction. This may account for the fact that the solvent exchange characteristics of the imino proton of the 8•20 base pair are faster than those of the imino proton of the 9•18 base pair in the complex. The A19 residue can be replaced by guanine with no effect on the specificity and high affinity of complex formation.

Intermolecular contacts in the complex

Previous studies on neomycin inhibition of the hammerhead ribozyme have demonstrated the importance of ionic interactions for aminoglycoside–RNA complex formation [10]. We have looked for patterns of intermolecular contacts involving tobramycin NH_3^+ groups with the RNA in the seven distance-refined structures of the complex. On average, one to three NH_3^+ groups interact with backbone phosphates and additional contacts are observed to the N7 atoms of purines amongst the refined structures. Unfortunately, we have been unable to identify a consistent pattern of specific NH_3^+-phosphate ionic contacts amongst the seven refined structures at the current resolution of structure determination. We also looked for but were unable to find a consistent pattern of specific intermolecular contacts involving either the hydroxyl groups on the tobramycin or the 2′-hydroxyl groups on the RNA in the refined structures of the complex. There appears, however, to be shape complementarity between the tobramycin and its RNA binding pocket in the complex (Figs 7b and 9b).

Hairpin-loop conformation

The U12–A13–G14 segment of the hairpin loop of the RNA aptamer adopts a well-defined conformation in the distance-refined solution structures of the complex (Fig. 7a). The key features are stacking between purines A13 and G14 (Fig. 10d) and a pair of cross-strand hydrogen bonds across the loop (Fig. 10a). One of these hydrogen bonds involves the 2′-OH of U12 as donor and the N7 of G14 as acceptor with H–N distance of 1.90 Å±0.11 for six of the seven refined structures of the complex. This hydrogen bonding is supported by the 9.36 ppm 2′-OH chemical shift of U12 in the tobramycin–RNA aptamer complex (Fig. 2b) which is downfield from the 6.5 ppm value typical of 2′-OH protons in RNA [22,23] but has a value similar to a slowly exchanging 2′-OH resonance (9.34 ppm) identified in the AMP–RNA aptamer complex [24–26]. The other hydrogen bond involves the imino proton of U12 as donor and the phosphate at the G14–C15 step with a large variation in the H–O distances amongst the refined solution structures. It is striking that the same fold for the three-residue turn has been observed in the heptanucleotide anticodon hairpin loop (Fig. 10b) and the TψC hairpin loop of yeast $tRNA^{phe}$ [27,28]. An even more striking resemblance can be observed between the overall hairpin

loop of the present tobramycin–RNA aptamer complex and that of a phylogenetically conserved hexanucleotide hairpin loop in ribosomal RNA [29]. The U-turn motif and a looped-out pyrimidine base followed by a mismatch closure of the hexanucleotide loop are common features in both structures. The G14 residue can be replaced by adenine with no effect on the specificity and high affinity of tobramycin–RNA aptamer complex formation.

The U12–A13–G14 segment and looped-out C15 residue are flanked by formation of a well defined U11•U16 mismatch pair in the refined structures of the complex. The U11 and U16 bases pair through one of two possible Wobble pairing alignments as shown in Figure 9c. Wobble T•T and U•U mismatch pairings have been identified previously in nucleic acids in solution [30,31] and in the crystalline state [32,33]. There is extensive stacking amongst the loop bases and between the U11•U16 mismatch pair and the adjacent Watson–Crick U10•A17 stem base pair in the complex. The sugar H1′ proton of U16 (4.38 ppm) is shifted to high field since it is positioned directly over the purine ring of G14 in the complex.

RNA discrimination

Tobramycin binds with nanomolar affinity to the RNA aptamer under investigation [11]. It is of interest to probe whether the solution structure of the complex provides an insight into why this sequence was selected and why others might be excluded. We believe that some of the key factors in the recognition and discrimination are as follows. First, the dimensions of the major groove at the tobramycin binding site. It appears that the major groove width is defined by the pyrimidine•pyrimidine U11•U16 mismatch and the sharp turn at U12–A13–G14 segment which orients U12 in the complex. The bulged A19 residue which is partially displaced into the major groove, also contributes to the width of this groove. Second, the sequence composition and size of the hairpin loop. The tobramycin binding site encompasses the hairpin loop of the RNA aptamer and there appears to be a key requirement for the sequence to be U11–U12–A13–R14–N15– U16, where R has to be a purine and N can be any base. Third, the flap formed by residue 15. The looping out of C15 (or A15 following substitution) and wrapping around the substrate was a unique and unexpected feature of the complex. Fourth, the major groove base-pair edge at the binding site. The floor of the major groove at the tobramycin binding site consists of the sequential edges of the Watson–Crick G9•C18 and U10•A17 base pairs, the Wobble U11•U16 mismatch pair and the U12•phosphate interaction. This represents a defined and unique combination which could provide an optimal fit for the bound tobramycin. The fifth and final factor likely to be central to recognition and discrimination is the specific intermolecular contact involving NH_3^+ and OH protons on tobramycin and phosphate, purine N7 and uracil O4 base edges and 2′-OH protons on RNA. The ensemble of solution structures of the complex do not provide consistent intermolecular contacts involving these groups, but these could emerge from a higher resolution structure determination of the complex. An effort is under way to achieve this goal on the basis of structural studies of a related tobramycin–RNA aptamer complex [11] currently under investigation in our laboratory.

Significance

Our knowledge of aminoglycoside antibiotic–RNA recognition to date has been restricted to the identification of binding sites for these saccharide antibiotics on ribosomal, catalytic intron, ribozyme and viral RNAs [5–10]. The aminoglycosides bind RNA with high affinity and specificity, with the RNA binding pockets discriminating between closely related family members. Our present study has defined structural features associated with the binding of tobramycin to a stem–loop junction in an RNA aptamer identified through *in vitro* selection [11]. The tobramycin binds site-specifically to the RNA major groove, and a significant segment of the antibiotic is encapsulated between the floor of the major groove and a looped-out cytosine residue that forms a flap over the binding pocket. We have been unable to identify specific ionic contacts between the charged NH_3^+ groups on the tobramycin and phosphates on the RNA aptamer that would represent common recognition elements amongst all the refined structures of the complex at the current resolution. Although the present study greatly expands our knowledge of saccharide–RNA recognition, still higher resolution data are required in order to identify potential specific intermolecular contacts at the interface of the complex. We have observed common features in the RNA conformation between the tip of the hairpin loop of the RNA aptamer in the tobramycin complex reported in this study and the tip of the anticodon and TψC hairpin loops in yeast $tRNA^{phe}$ [27,28]. Indeed, there are striking similarities in the fold of our hexanucleotide hairpin-loop conformation in the tobramycin–RNA aptamer complex and the fold reported for a phylogenetically conserved hexanucleotide loop in ribosomal RNA [29]. This suggests that the binding site for tobramycin characterized in this study may represent a recurring scaffold for aminoglycoside antibiotic-binding sites on natural RNA sequences.

Materials and methods

Sample preparation

The 27-mer RNA aptamer and its single base-substitution analogs were prepared either by chemical synthesis on an Applied Biosystems synthesizer or by *in vitro* transcription using T7 transcription and synthetic DNA templates [34,35]. The RNA oligomers were ethanol precipitated and purified using 20% denaturing polyacrylamide-gel electrophoresis (containing 7 M urea). The RNA oligomer was monitored by UV shadowing, cut and electroeluted using an elutrap (Schleicher and Schuell, Inc). The eluted RNA was ethanol-precipitated and equilibrated with NMR buffer (10 mM phosphate, pH 6.8) by spinning through an Amicon centricon (3 kDa cut off), with the procedure repeated five to seven times. A 50 ml transcription yields about 15 mg of RNA. The same transcription

conditions were used for uniformly ^{13}C,^{15}N-labeled RNA except that ^{13}C and ^{15}N-labeled nucleoside triphosphates (NTPs) were used instead of unlabeled counterparts. The ^{13}C,^{15}N-labeled NTPs were isolated from an *Escherichia coli* strain overexpressing ribosomal RNA grown in minimum medium containing ^{13}C glucose and ^{15}N ammonium sulfate as carbon and nitrogen sources [36].

A tobramycin (Fluka, NY) stock solution (100 mM) was prepared by dissolving the antibiotic in an aqueous solution adjusted to pH 6.8. This stock solution was gradually added to the RNA aptamer and complex formation followed by recording imino proton spectra.

NMR spectroscopy

NMR spectra were collected on Varian Unity Plus 600 MHz and 500 MHz NMR spectrometers. A detailed description of the multinuclear multidimensional NMR experiments used for data collection have been outlined in previous publications from our laboratory on ligand–RNA aptamer complexes [25,37]. The NMR data were processed on SUN work stations using VNMR software and analyzed using the FELIX program (Molecular Simulations Inc). The three-dimensional NMR data were processed using NMRPipe and PIPP programs [38,39]. Proton chemical shifts were referenced to 2,2-dimethyl-2-silapentane-5-sulfonate (DSS) while carbon and nitrogen chemical shifts were indirectly referenced to DSS and ammonia, respectively.

Input restraints

Input distance restraints involving nonexchangeable protons were derived from NOE build-up experiments in NOESY spectra on the complex recorded at mixing times of 50, 100, 150 and 200 ms in D_2O buffer at 25°C. The volume integrals of each non-overlapped cross-peak were measured and plotted against the mixing time as build-up curves and fitted to second-order polynomials. Inter-proton distances were calculated from the initial build-up rates using the slopes of the cytosine and uracil H5–H6 intra-residue cross-peaks as a reference, calibrated to a 2.45 Å distance. The distance restraints were assigned an upper and lower bounds range of 15% for well-resolved cross-peaks, 25% for slightly overlapped cross-peaks, 30% for cross-peaks involving adenine H2 protons and 40% for significantly overlapped cross-peaks. In addition, very weak cross-peaks in 300 ms mixing time NOESY spectra were given upper bounds of 6.5 Å. Interproton distance restraints involving exchangeable protons in the complex were derived from NOESY spectra recorded at 100 and 200 ms mixing times in H_2O buffer at 5°C. The inter-proton distances were calibrated against the uracil imino to adenine H2 distance of 2.93 Å as reference. The distance restraints were assigned an upper and lower bounds range of 25%, which was increased to 35% for restraints involving amino protons. Additional restraints were obtained from analysis of cross-peaks in a NOESY–HMQC data set on the complex recorded at a mixing time of 120 ms in D_2O buffer at 25°C. These restraints were treated in a more qualitative manner and classified as strong (2.65 Å ± 0.85), medium (3.40 Å ± 1.60) or weak (4.15 Å ± 2.35).

Watson–Crick pairing alignments were imposed for the duplex portion of the RNA (residues 1–8 and 20–27) in the initial stages of the calculations and for the short stem segment (residues 9–10 and 17–18) in the later stages of the calculations. These hydrogen–heavy atom distances were taken from the standard base-pair geometries of nucleic acids [40] and were assigned values of 2.0 Å ± 0.2. The backbone of the first four base-pairs (G1–A4 and U24–C27) of the longer duplex stem was restricted to that of A-form duplex RNA during the computations.

A few sugar pucker restraints were used based on an analysis of phase-sensitive–COSY spectra of the complex in D_2O buffer at 25°C. The presence of strong H1′–H2′ coupling cross-peaks was interpreted as C2′-endo family of sugar puckers, whereas the absence of H1′–H2′coupling cross-peaks were interpreted as C3′-endo family of sugar puckers and translated to the corresponding values and ranges for the sugar endocyclic torsion angles [40]. Residues G1, A17, C18 and C27 which exhibit weak to medium intensity H1′–H2′ coupling cross-peaks were excluded from the the C3′-endo pucker range and restricted to values of P = 108°–216°. All other residues were left unrestrained during the computations.

The six-membered rings of tobramycin were restricted to a chair pucker early in the computations but this restriction was released at later stages in the computations on the complex.

Starting structures of the complex

The starting structure of tobramycin was generated using the INSIGHT program with the III–I linkage defined by the torsion angles III(H1″)–III(C1″)–O–I(C6) = −7.8° and III(C1″)–O–I(C6)–I(H6) = −2.4°, while the I–II linkage was defined by the torsion angles I(H4)–I(C4)–O–II(C1′) = −12.0° and I(C4)–O–II(C1′)–II(H1′) = 1.9°. The starting structure of the RNA aptamer was A-form in the stem, bulge and loop regions. Watson–Crick base pairing was maintained in the (G1–G8)•(C20–C27) stem segment throughout the calculations and introduced at the (G9–U10)•(A17–C18) stem segment at a later stage in the calculations. The tobramycin molecule was placed in a randomized orientation at the center of mass of the RNA to generate 50 starting structures of the complex.

Distance-restrained molecular dynamics simulations

Restrained molecular dynamics calculations were performed on the tobramycin-RNA aptamer complex on the basis of on a simulated annealing protocol in vacuum with a distance-dependent dielectric constant using the X-PLOR program [41]. All intermolecular nonbonded interactions were turned off during the initial stages of the refinement. The system was heated to 1000 K and then maintained at this temperature over a period of 230 ps, during which all distance restraints were added in a gradual manner, with shorter range restraints added first followed by increasingly longer range restraints in terms of the primary sequence of the system. A single weak restraint was initially employed between tobramycin and the RNA aptamer, to prevent the molecules from migrating apart during the simulation. The weights for both distance and dihedral restraints were grown to a value of 100 kcal mol^{-1} $Å^{-2}$ and 100 kcal mol^{-1} rad^{-2}, respectively, during this period. The molecular dynamics calculations were continued at 1000K for another 20 ps followed by cooling from 1000 K to 50 K over 20 ps and subsequent minimization. The nonbonded interactions between tobramycin and the RNA were added during the second phase of the refinement. The van der Waals interaction between molecules was introduced gradually in cycles of minimization, with the weight of this term growing from 10^{-10} to 1. This was followed by 5 ps of molecular dynamics at 200K. The electrostatics term between molecules was next gradually introduced in cycles of dynamics with the weight of this term growing from 10^{-10} to 1. The system was then cooled from 200K to 50K during 20 ps of dynamics followed by minimization. The resulting structures were heated to 300 K and retained at this temperature for 20 ps with all restraints involving A19 base protons initially turned off and then grown in during this period. This was done in an attempt to better characterize the position of A19 in the complex. The dynamics was continued for an additional 20 ps, during which the system was cooled from 300 K to 50 K, followed by minimization. Seven best structures of the complex were selected for analysis based on the lowest NOE violations, acceptable covalent geometry and favorable van der Waals energy.

Structure analysis

The helical parameters of the RNA were analyzed using the CURVES program [42]. Color figures were prepared using the INSIGHTII program (Molecular Simulations Inc.) and the GRASP program [43].

Coordinates deposition

The coordinates of the tobramycin–RNA aptamer complex (accession number: 1TOB) have been deposited with the Protein Data Bank, Brookhaven National Laboratory, Upton, New York, 11923, USA, from whom copies can be obtained.

Supplementary material

Supplementary material published with this paper on the internet includes: two tables of proton and carbon chemical shifts of tobramycin and RNA aptamer protons and carbons in the tobramycin–RNA aptamer complex and seventeen figures of NMR data on the tobramycin–RNA aptamer complex in H_2O and D_2O solution.

Acknowledgements

This research was funded by NIH grant GM 54377 to DJP. We thank Weijun Xu for preparation of the T7 polymerase and uniformly labeled ^{13}C,^{15}N nucleoside triphosphates; David Live for his help with NMR data collection and processing and John Hubbard for help in the preparation of color figures. Multinuclear multidimensional NMR software was kindly provided by Frank Delaglio and Daniel Garrett of the Laboratory of Chemical Physics, NIDDK, NIH.

References

1. Tanaka, N. (1965). Aminoglycoside antibiotics. Antibiotics III: mechanism of action of antimicrobial and antitumor agents (Corcoran, J.W. & Hahn, F.E. eds), pp. 340–364, Springer-Verlag, Berlin, Germany.
2. LeGoffic, F., Capmau, M.L., Tangy, F. & Baillarge, M. (1979). Mechanism of action of aminoglycoside antibiotics. *Eur. J. Biochem.* **102**, 73–81.
3. Gale, E.F., Cundliffe, E., Reynolds, P.E., Richmond, M.H. & Waring, M.J. (1981). *The Molecular Basis of Antibiotic Action*. pp. 402–547, John Wiley & Sons, London, UK.
4. Cundliffe, E. (1987). On the nature of antibiotic binding sites in ribosomes. *Biochimie* **69**, 863–869.
5. Moazed, D. & Noller, H.F. (1987). Interaction of antibiotics with functional sites in 16S ribosomal RNA. *Nature* **327**, 389–394.
6. Recht, M.I., Fourmy, D., Blanchard, S.C., Dahlquist, K.D. & Puglisi, J.D. (1996). RNA sequence determinants for aminoglycoside binding to an A-site rRNA model oligonucleotide. *J. Mol. Biol.* **262**, 421–436.
7. von Ahsen, U., Davies, J. & Schroeder, R. (1991). Antibiotic inhibition of group I ribozyme function. *Nature* **353**, 368–370.
8. von Ahsen, U. & Noller, H.F. (1993). Footprinting the sights of interaction of antibiotics with catalytic group I intron RNA. *Science* **260**, 1501–1503.
9. Zapp, M.L., Stern, S. & Green, M.R. (1993). Small molecules that selectively block RNA binding of HIV-1 rev protein inhibit rev function and viral production. *Cell* **74**, 969–978.
10. Clouet-d'Orval, B., Stage, T.K. & Uhlenbeck, O.C. (1995). Neomycin inhibition of the hammerhead ribozyme involves ionic interactions. *Biochemistry* **34**, 11186–11190.
11. Wang, Y. & Rando, R.R. (1995) Specific binding of aminoglycoside antibiotics to RNA. *Chemistry & Biology* **2**, 281–290.
12. Lato, S.M., Boles, A.R. & Ellington, A.D. (1995). *In vitro* selection of RNA lectins: using combinatorial chemistry to interpret ribozyme evolution. *Chemistry & Biology* **2**, 291–303.
13. Wallis, M. G., von Ahsen, U., Schroeder, R. & Famulok, M. (1995). A novel RNA structure for neomycin recognition. *Chemistry & Biology* **2**, 543–552.
14. Del Bene, V.E., & Farrar, Jr., W.E. (1972). Tobramycin: *in vitro* activity and comparison with kanamycin and gentamicin. *Antimicr. Ag. Chemoth.* **1**, 340.
15. Fiala, R., Jiang, F. & Patel, D.J. (1996). Direct correlation of exchangeable and nonexchangeable protons in purine bases in ^{13}C,^{15}N-labeled RNA using HCCNH-TOCSY experiment. *J. Am. Chem. Soc.* **118**, 689–690.
16. Simorre, J.P., Zimmermann, G.R., Mueller, L. & Pardi, A. (1996). Correlation of guanosine exchangeable and nonexchangeable protons in ^{13}C-/^{15}N-labeled RNA with an HNC-TOCSY-CH experiment. *J. Biomol. NMR* **7**, 153–156.
17. Sklenar, V., Dieckmann, T., Butcher, S.E. & Feigon, J. (1996). Through bond correlation of imino and aromatic resonances in ^{13}C,^{15}N-labeled RNA via heteronuclear TOCSY. *J. Biomol. NMR* **7**, 83–87.
18. Patel, D.J., Kozlowski, S.A., Nordheim, A. & Rich, A. (1982). Right-handed and left-handed DNA: studies of B-DNA and Z-DNA by using proton nuclear Overhauser effect and phosphorus NMR. *Proc. Natl. Acad. Sci. USA.* **79**, 1413–1417.
19. van Pelt, J.E., Moobery, E.S. & Frey, P.A. (1990). ^{1}H, ^{13}C and ^{31}P NMR spectral assignments of tobramycin, 2″-(adenosine-5′-phosphoryl)-tobramycin and 2″-(adenosine-5′-thiophosphoryl)-tobramycin. *Arch. Biochem. Biophys.* **280**, 284–291.
20. Koyima, G., Iitaka, Y., Maeda, K. & Umezawa, H. (1968). The crystal structure of kanamycin. *Tetrahedron Lett.* **15**, 1875–1879.
21. Pedersen, L.C., Benning, M.M. & Holden, H.M. (1995). Structural investigation of the antibiotic and ATP-binding sites in kanamycin nucleotidyltransferase. *Biochemistry* **34**, 13305–13311.
22. Cheong, C., Varani, G. & Tinoco, Jr. I. (1990). Solution structure of an unusually stable RNA hairpin, 5′-GGAC(UUCG)GUCC. *Nature* **346**, 680–682.
23. Allain, F.H.T. & Varani, G. (1995). Structure of the P1 helix from group I self-splicing introns. *J. Mol. Biol.* **250**, 333–353.
24. Jiang, F., Kumar, R.A., Jones, R. & Patel, D.J. (1996). Structural basis of RNA folding and recognition in an AMP–RNA aptamer complex. *Nature* **382**, 183–186.
25. Jiang, F., Fiala, R., Live, D., Kumar, R.A. & Patel, D.J. (1996). RNA folding topology and intermolecular contacts in the AMP–RNA aptamer complex. *Biochemistry* **40**, 13250–13266.
26. Dieckmann, T., Suzuki, E., Nakamura, G. K. & Feigon, J. (1996). Solution structure of an ATP-binding RNA aptamer reveals a novel fold. *RNA* **2**, 628–640.
27. Kim, S.H., *et al.*, & Rich, A. (1974). Three-dimensional tertiary structure of yeast phenylalanine transfer RNA. *Science* **185**, 435–439.
28. Robertus, J.D., *et al.*, & Klug, A. (1974). Structure of yeast phenylalanine tRNA at 3 Å resolution. *Nature* **250**, 546–551.
29. Huang, S., Wang, Y-X. & Draper, D.E. (1996). Structure of a hexanucleotide RNA hairpin loop conserved in ribosomal RNAs. *J. Mol. Biol.* **258**, 308–321.
30. Kouchakdjian, M., Li., B.F., Swann, P.F. & Patel, D.J. (1988). Pyrimidine–pyrimidine base pair mismatches in DNA: an NMR study of T•T pairing at neutral pH and C•C pairing at acidic pH in dodecnucleotide duplexes. *J. Mol. Biol.* **200**, 139–155.
31. Wang, Y-X., Huang, S. & Draper, D.E. (1996). Structure of a U•U pair within a conserved ribosomal RNA hairpin. *Nucleic Acids Res.* **24**, 2666–2672.
32. Bayens, K.J., De Bondt, H.L. & Holbrook, S.R. (1995). Structure of an RNA double helix including uracil–uracil base pairs in an internal loop. *Nat. Struct. Biol.* **2**, 56–62.
33. Rould, M.A., Perona, J.J. & Steitz, T.A. (1991). Structural basis of anticodon loop recognition by glutaminyl-tRNA synthetase. *Nature* **352**, 213–218.
34. Milligan, J.F., Groebe, D.R., Witherall, G.W. & Uhlenbeck, O.C. (1987). Oligoribonucleotide synthesis using T7 RNA polymerase and synthetic DNA templates. *Nucleic Acids Res.* **15**, 8783–8798.
35. Wyatt, J.R., Chastain, M. & Puglisi, J.D. (1991). Synthesis and purification of large amounts of RNA oligonucleotides. *Biotechniques* **11**, 764–769.
36. Nikonowicz, E.P., Sirr, A., Legault, P., Jucker, F.M., Baer, L.M. & Pardi, A. (1992). Preparation of ^{13}C and ^{15}N labeled RNAs for heteronuclear multi-dimensional NMR studies. *Nucleic Acids Res.* **20**, 4508–4513.
37. Fan, P., Suri, A.K., Fiala, R., Live, D., & Patel, D.J. (1996). Molecular recognition in the FMN–RNA aptamer complex. *J. Mol. Biol.* **258**, 480–500.
38. Delaglio, F., Grzesiek, S., Vuister, G., Zu, G., Pfeiffer, J. & Bax, A. (1995). NMRPipe: a multidimensional spectral processing system based on UNIX pipes. *J. Biomol. NMR* **6**, 277–293.
39. Garrett, D.S., Powers, R., Gronenborn, A.M. & Clore, G.M. (1991). A common sense approach to peak picking in two, three and four-dimensional spectra using automatic computer analysis of contour programs. *J. Magn. Reson.* **95**, 214–220.
40. Saenger, W. (1984). *Principles of Nucleic Acid Structure*. Springer-Verlag, New York.
41. Brünger, A.T. (1992). X-PLOR User Manual. (Version 3.1), Yale University, New Haven.
42. Lavery, R. & Sklenar, H. (1988). The definition of generalized helicoidal parameters and axis of curvature for irregular nucleic acids. *J. Biomol. Struct. Dyn.* **6**, 63–91.
43. Nicholls, A., Sharp, K.A. & Honig, B.H. (1991). Protein folding and association: insights from the interfacial and thermodynamic properties of hydrocarbons. *Proteins* **11**, 281–296.